THE JOURNAL OF PHYSICAL CHEMISTRY B

Article

pubs.acs.org/JPCB

Solvent-Independent Anharmonicity for Carbonyl Oscillators

Samuel H. Schneider,[†] Huong T. Kratochvil,[‡,⊥] Martin T. Zanni,*[,‡] and Steven G. Boxer*[,†]

[†]Department of Chemistry, Stanford University, Stanford, California 94305-5012, United States

[‡]Department of Chemistry, University of Wisconsin—Madison, Madison, Wisconsin 53706, United States

Supporting Information

ABSTRACT: The physical origins of vibrational frequency shifts have been extensively studied in order to understand noncovalent intermolecular interactions in the condensed phase. In the case of carbonyls, vibrational solvatochromism, MD simulations, and vibrational Stark spectroscopy suggest that the frequency shifts observed in simple solvents arise predominately from the environment's electric field due to the vibrational Stark effect. This is contrary to many previously invoked descriptions of vibrational frequency shifts, such as bond polarization, whereby the bond's force constant and/or partial nuclear charges are altered due to the environment, often illustrated in terms of favored resonance structures. Here we test these hypotheses using vibrational solvatochromism as measured using 2D IR to assess the solvent dependence of the bond anharmonicity. These results indicate that the carbonyl bond's anharmonicity is independent of solvent as tested using hexanes, DMSO, and D_2O and is supported by simulated 2D spectra. In support of the linear vibrational Stark effect, these 2D IR measurements are consistent with the assertion that the Stark tuning rate is unperturbed by the electric field generated by both hydrogen and non-hydrogen bonding environments and further extends the general applicability of carbonyl probes for studying intermolecular interactions.

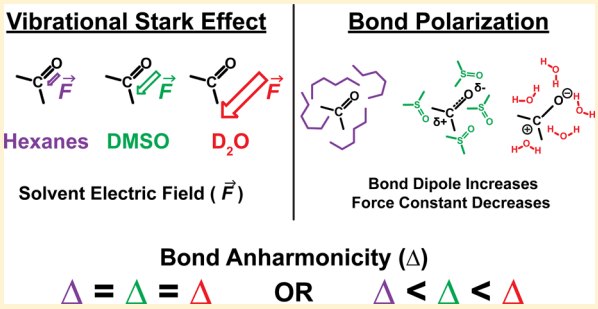

INTRODUCTION

Solvatochromism is the familiar effect of solvent polarity on color, typically of dye molecules.[1−4] This effect is primarily due to the interaction between the solvent electric field and the change in dipole moment between the ground and excited states of the dye, $|\Delta\vec{\mu}|$, referred to as the Stark tuning rate. Vibrational solvatochromism is less familiar, with some of the earliest work dating back to Badger and Bauer correlating frequency shifts to hydrogen bonding strength,[5] but has been studied more systematically recently because it provides a basis for calibrating electric fields in condensed-phase systems and a connection with the vibrational Stark effect (VSE).[6] An example is shown in Figure 1A for the carbonyl group of acetophenone, where a systematic red shift to lower wavenumbers is associated with increasing solvent polarity; in addition, the width of the transition increases systematically with solvent polarity. As described in several papers, the electric field sensed by the carbonyl group in fluid solution can be calculated using MD simulations employing either fixed charge[7−10] or polarizable force fields[11] for a range of solvents. The results for acetophenone are plotted in Figure 1B, showing an excellent linear correlation between the observed carbonyl peak frequency and the calculated average value of the electric field projected onto the carbonyl probe, $|\langle F_{C=O}\rangle|$, for both hydrogen bonding (H-bonding) and non-H-bonding solvents. A similar correlation is observed for the line width, suggesting that it is largely inhomogeneous and due to the distribution of fields in fluid solution and in the simulations. The slope of the best-fit line corresponds to the Stark tuning rate, $|\Delta\vec{\mu}_{C=O}|$, which can be measured independently in frozen glasses by vibrational Stark spectroscopy,[7] $|\Delta\vec{\mu}_{C=O}|f$ (where f is the local field correction of ∼2),[12] providing further evidence that the correlation has validity. Other more sophisticated multiparameter fitting methods have been introduced that also show that the effects are largely electrostatic in origin, and this is the primary application of these fits.[10,13−15]

An essential assumption of this analysis and applications of this frequency-to-field conversion (dashed lines in Figure 1B) for carbonyl probes in more complex environments, such as enzyme active sites,[7−9,16] is that $|\Delta\vec{\mu}_{C=O}|$ is an intrinsic property of the oscillator, independent of its environment. The calculations giving $|\langle F_{solv}\rangle|$ and leading to the excellent correlation in Figure 1B keep the properties of the probe bond fixed and treat the electric field from the solvent using classical electrostatics, that is, the shifts are linear VSEs. Another way to view this idea is that the bond anharmonicity and accompanying displacement of charge for the $\nu = 0 \rightarrow 1$ transition, which is responsible for $|\Delta\vec{\mu}_{C=O}|$ ($|\Delta\vec{\mu}| = 0$ for a harmonic oscillator), are independent of solvent polarity (Figure 2A). This can be modeled with the Morse potential[17] and linear VSE to map the vibrational potential energy surface and corresponding transitions

Received: January 17, 2017
Revised: February 22, 2017
Published: February 22, 2017

ACS Publications © 2017 American Chemical Society

DOI: 10.1021/acs.jpcb.7b00537
J. Phys. Chem. B 2017, 121, 2331−2338

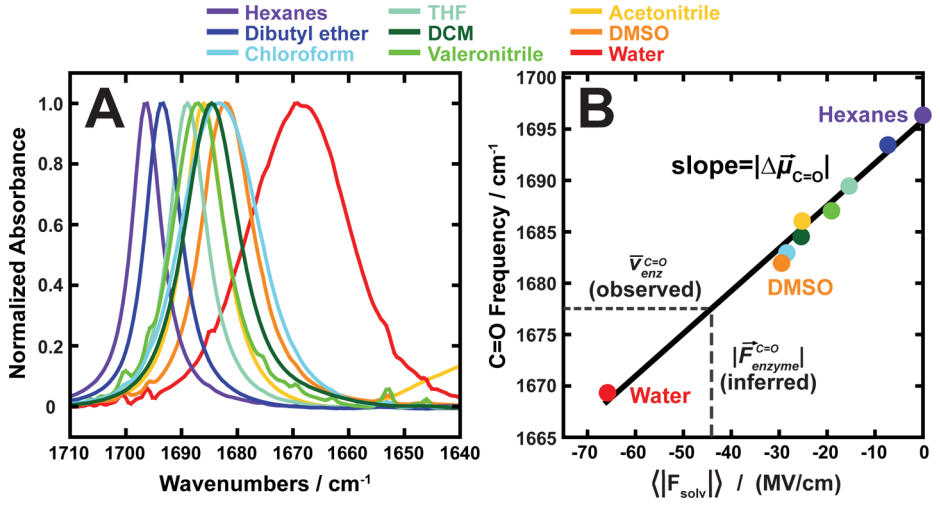

Figure 1. C═O vibrational solvatochromism due to the solvent electric field for acetophenone. (A) Normalized FTIR spectra of the carbonyl vibration of acetophenone (10 mM) dissolved in organic solvents and water (D_2O). The spectra are colored from violet to red in order of increasing static dielectric constant. (B) Linear correlation between the C═O stretching frequency and the average electric field experienced by the bond in acetophenone as calculated from MD simulations. The linear least-squares regression model is $\bar{\nu}_{C=O} = 0.414\langle|F_{solv}|\rangle + 1695.7$ with $R^2 = 0.99$, where the slope 0.414 $cm^{-1}/(MV/cm)$ corresponds to the Stark tuning rate, $|\Delta\vec{\mu}_{C=O}|$. This calibration curve can be utilized to convert from an observed frequency shift, for example, in an enzyme active site, $\bar{\nu}_{enz}^{C=O}$, to an inferred electric field, $\vec{F}_{enz}^{C=O}$ (dashed lines). Figure adapted from Fried et al.[7]

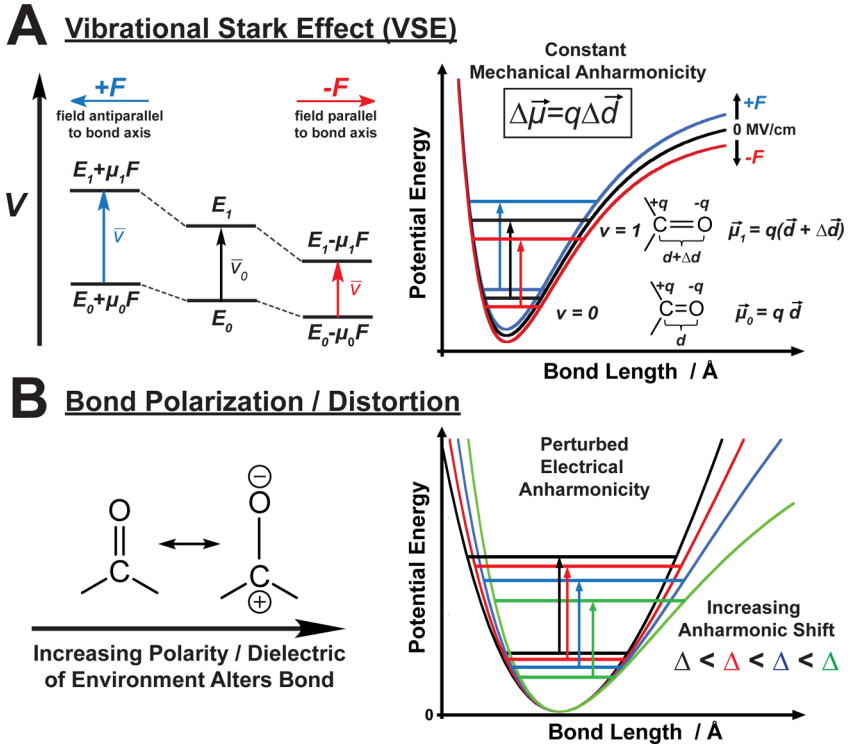

Figure 2. Models for vibrational solvatochromism. (A) VSE in an external electric field $\vec{F}_{ext}$ used to measure the linear Stark tuning rate, $|\Delta\vec{\mu}_{C=O}|$, which defines how a bond interacts with an electric field through the mechanical anharmonicity. When placed in different solvents, the Stark tuning rate probes the solvent electric field, but the bond anharmonicity, and thus force constant, remains fixed. (B) The possible effect of solvent polarity on bond order is reflected in a change in anharmonicity. The mechanism by which frequency shifts arise from a change in the bond character or resonance form of the bond as a function of different environments. In this scenario, the bond anharmonicity changes with solvent electric field, denoted in terms of increasing anharmonic shifts (Δ) as the bond "weakens" due to changes in the atomic charges, bond length, and force constant.

$$V(\vec{d}) = D_e[1 - e^{-\alpha(|\vec{d}|-|\vec{d}|_e)}]^2 - (q\vec{d})\cdot\vec{F} \quad (1)$$

$$\bar{\nu}_{01} = \omega_0 - 2\omega_0\chi_e - (q\Delta\vec{d})\cdot\vec{F} \quad (2)$$

where D_e is the well-depth of the potential (cm^{-1}, not to be confused with the dissociation energy D_0), α is the width of the potential (cm^{-1}), $\vec{d}_e$, $\vec{d}$, and $\Delta\vec{d}$ are the equilibrium bond distance, internuclear distance, and change in distance between the ground and excited state, respectively, q is the bond's effective charge, and $\vec{F}$ is the matrix electric field. The parameters, D_e and α, are related to the anharmonicity constant (χ_e) and are determined from the following relations[18]

DOI: 10.1021/acs.jpcb.7b00537
J. Phys. Chem. B 2017, 121, 2331−2338

$$\chi_e = \frac{\bar{\nu}_{01} - \bar{\nu}_{12}}{2\omega_0} = \frac{\bar{\nu}_{01} - \bar{\nu}_{12}}{2(2\bar{\nu}_{01} - \bar{\nu}_{12})} \quad (3)$$

$$D_e = \frac{\omega_0}{4\chi_e} \quad (4)$$

$$\alpha = \left(\frac{8\pi^3 m \chi_e \omega_0 c}{100h}\right)^{1/2} \quad (5)$$

where the $\bar{\nu}$ correspond to the vibrational frequencies in cm^{-1} and the subscript corresponds to the observed vibrational transition (i.e., $0 \rightarrow 1$ or $1 \rightarrow 2$), ω_0 is the harmonic frequency (cm^{-1}) based on the harmonic oscillator approximation in the gas phase, h is Planck's constant, c is the speed of light (m s^{-1}), m is the reduced mass (kg), and χ_e is the cubic anharmonicity constant (unitless). The linear VSE assumes that ω_0, q, $|\Delta\vec{d}|$, and χ_e are constant across different environments, as depicted in Figure 2A. Ab initio calculations that model the effect of an electric field on the carbonyl bond in vacuum suggest that there is a linear Stark effect up to fields as large as about 150 MV/cm, at which point the field begins to affect the bonding.[9,19] Likewise, solution simulations in which the probe bond polarizability was included are also consistent with a linear Stark effect.[20]

An alternative interpretation for the change in frequencies of a vibrational mode is a change in the bond force constant, for example, a more red-shifted peak corresponds to a weaker bond, often highlighted with arrows to describe the stabilizing effect of a more polar solvent on resonance structures with weaker bonds (Figure 2B). This effect is sometimes called "bond polarization" and has been widely used to rationalize frequency shifts in condensed-phase systems.[21−23] The bond polarization effect would be expected to alter the vibrational potential and energy levels according to the Morse potential

$$V(\vec{d}) = D_e[1 - e^{-\alpha(|\vec{d}|-|\vec{d}_e|)}]^2 \quad (6)$$

$$\bar{\nu}_{01} = \omega_0 - 2\omega_0\chi_e \quad (7)$$

whereby χ_e and/or q would be expected to change based on the solvent, thus resulting in different values of D_e, ω_0, and $|\Delta\vec{d}|$, as depicted in Figure 2B. Likewise, it has been generally observed that there is a correlation between bond length and frequency shifts,[24−26] which has also been argued in support of bond polarization. The VSE can also explain bond polarization in terms of the difference polarizability,[11] which is generally assumed to be small for vibrational transitions,[6,27−29] suggesting that these solvatochromic shifts can be explained primarily as linear Stark effects.

Thus, there are two competing limiting interpretations, corresponding to very different physical phenomena, for the solvatochromism of vibrational modes, where our focus is on largely isolated high-frequency modes, for example, C═O and C≡N. One can distinguish between these two mechanisms by measuring the bond anharmonicity. This measurement is common in the gas phase by measuring overtone and combination bands but less common in condensed phases largely because these transitions are weak and often overwhelmed by modes from the solvent.[30] While the vibrational Stark spectrum of acetophenone and other carbonyl probes in a mixed frozen solvent where both H-bonded and non-H-bonded forms are present can be fit with a single $|\Delta\vec{\mu}_{C=O}|f$,[7,8] 2D IR can provide a more direct measurement of the anharmonicity in fluid solution because both the $\nu = 0 \rightarrow 1$ ($\bar{\nu}_{01}$) diagonal peak and the $\nu = 1 \rightarrow 2$ ($\bar{\nu}_{12}$) off-diagonal peak are readily observed. The anharmonic shift, Δ, is given by subtracting the frequencies of the $\nu = 0 \rightarrow 1$ and $\nu = 1 \rightarrow 2$ peaks, for example, $\Delta = \bar{\nu}_{01} - \bar{\nu}_{12}$. The limiting cases illustrated in Figure 2 predict that Δ would be constant with solvent polarity if spectral shifts were due to the linear VSE (Figure 2A), while a bond polarization mechanism would predict that Δ should increase with solvent polarity as the bond is weakened (Figure 2B).

In order to test the solvent dependence of the anharmonicity, the anharmonic shifts of several carbonyl oscillators dissolved in hexanes, DMSO, and D_2O have been studied using 2D IR. Hexanes and D_2O represent the two extremes of the general solvatochromic series, with significantly different polarities, dielectric constants, and intermolecular interactions (i.e., H-bonding and non-H-bonding), while DMSO was selected due to its intermediate polarity, miscibility with all solutes, and because it has been used in previous measurements of carbonyl anharmonicities.[31,32] This work indicates that the carbonyl anharmonicity is constant across these different solvent environments, supporting the notion that the Stark tuning rate is an intrinsic property of carbonyl vibrational probes. These results have important implications for interpreting vibrational frequency shifts in the condensed phase.

MATERIALS AND METHODS

2D IR Spectroscopy. The 800 nm output of a 3.5 W, 100 fs regenerative amplifier was used to pump an OPA to generate signal and idler wavelengths. The signal and idler were focused into a $AgGaS_2$ crystal (Type II, $\theta = 42°$) in a difference frequency generation setup to generate mid-IR centered at around 6 μm. A CaF_2 beamsplitter splits the mid-IR into probe and pump pulses. The pump pulse is subsequently shaped in the frequency domain using a Ge AOM based pulse shaper, as previously described.[33,34] The pump and probe pulses are then focused onto the sample where the signal was focused onto the slit of a commercial monochromator and detected using a 2 × 64 element MCT array.

Simulations and Fitting. For nearly all compounds in the condensed phase, the diagonal anharmonic shift is smaller or comparable to the line widths. As a result, the $0 \rightarrow 1$ (negative intensity) and $1 \rightarrow 2$ (positive intensity) peaks in a 2D IR spectrum will partially overlap and destructively interfere, causing the frequency separation between the $0 \rightarrow 1$ and $1 \rightarrow 2$ peaks to appear larger than the true anharmonic shifts (Figure S2, Table S2).[35] As such, we extract the true anharmonic shifts through fits to the pump slices taken along the pump frequency with the minimum $0 \rightarrow 1$ intensity for each solute−solvent pair. The pump slices were fit using two Voigt line shapes implemented in Origin 2016 to extract the relevant data. Using nonlinear curve fitting and the orthogonal distance regression algorithm, the pump slice of each solute−solvent pair, normalized to the fundamental mode, was fit to two line shapes, each represented with a Voigt profile. For a given solute, the Lorentzian line width was assumed to be constant across all solvents for both the fundamental ($0 \rightarrow 1$) and $1 \rightarrow 2$ transition, as supported by the constant antidiagonal line widths.[35] The fundamental transition was fit with two adjustable parameters (peak area and Gaussian line width), while the $1 \rightarrow 2$ transition was fit to three adjustable parameters (anharmonic shift, peak area, and Gaussian line width). The frequency and the fwhm of the $0 \rightarrow 1$ transition were constrained to the values determined from linear IR measure-

DOI: 10.1021/acs.jpcb.7b00537
J. Phys. Chem. B 2017, 121, 2331−2338

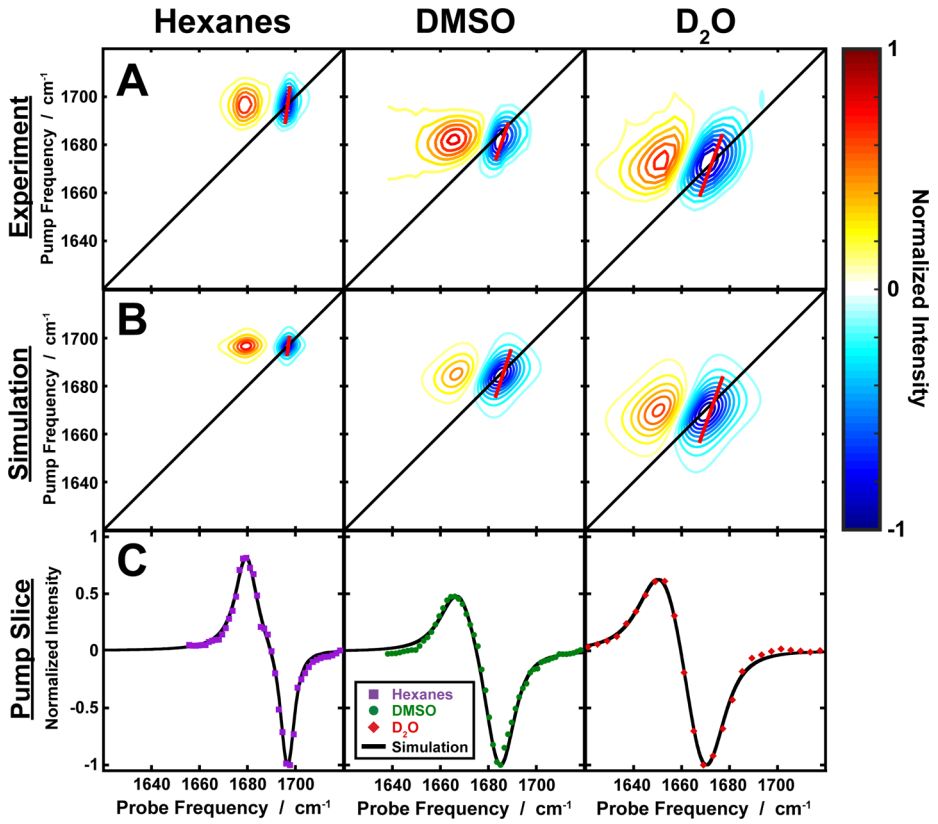

Figure 3. Experimental and simulated 2D IR spectrum of acetophenone in hexanes, DMSO, and D_2O. (Row A) Experimental 2D IR spectra and (row B) simulated spectra using fixed anharmonicity and population relaxation (T_1). The fundamental (blue) and 1 → 2 (red) transition are shown for each spectra, with CLSs shown in red. Details of the CLS fitting and 2D simulated spectra are described in the Materials and Methods section. (Row C) Overlay of the pump slices from experiment (purple squares, green circles, red diamonds) and best fit from simulation (solid black lines) along the peak maximum for different solvents. Experimental and simulated line shape parameters are reported in Table S3.

ments. However, due to the resolution of the 2D IR measurements and the increasing center line slope (CLS) in polar solvents, the peak position will shift if the pump slice is not directly at the frequency of the peak maxima as determined from linear measurements. As such, the peak position was constrained to allow an uncertainty of ±3 cm^{-1} from the center frequency determined by linear IR, and comparison of the peak positions from fits to the pump slices and the linear IR measurements are in good agreement (Table S1). The parameters in the 1 → 2 fitting were constrained to ensure that $fwhm_{12}$ > $fwhm_{01}$, as expected due to the population relaxation (T_1) contribution to the homogeneous dephasing.[35] Confidence intervals (CIs) for each parameter were determined at the 99% confidence level as calculated using Origin 2016. This was tested with two different gratings (75 and 150 g/mm) for the acetophenone measurements in hexanes and DMSO in order to increase resolution due to the narrow line widths of the C═O peak in these solvents (Figure S1).

CLSs were determined from experimental and simulated 2D spectra according to the CLSω_m method, which assumes Gaussian fluctuations.[36−39] In short, slices were taken parallel to the probe axis along the transition of interest (note that there are different conventions in the axes labeling in 2D IR such that $\omega_m = \omega_{probe}$ and $\omega_\tau = \omega_{pump}$ in this context), and the resulting spectrum was fit to a Gaussian line shape to find the peak maximum at each pump frequency. The CLS was then extracted from the slope as determined from plotting the probe frequency maximum as a function of the pump frequency.

We simulated the 2D spectra using a defined correlation function of the functional form shown in eq 8 and the necessary theoretical formalism[40]

$$C(t) = \Delta_0^2 e^{-t/\tau_0} + \Delta_1^2 \quad (8)$$

where t is the time in fs, τ_0 is the correlation time in fs, and Δ_0 and Δ_1 are the frequency fluctuation amplitudes in ps^{-1}. Δ_i magnitudes are the contribution to the line shape. Using the peak positions and anharmonic shift as determined by the 2D IR spectroscopic measurements and estimated T_1 population relaxation times of 1175, 2500, and 840 fs for acetophenone, methyl benzoate, and ethyl thioacetate, respectively, the time-dependent response functions for each of the rephasing and nonrephasing pathways were calculated and used to generate the simulated 2D IR spectra. The vibrational lifetimes (T_2) were in the generally observed range for other simple carbonyl compounds (0.8−5.2 ps[41−44]), though this has been tested predominately with amides. The relative intensities of the overtones were scaled in order to more closely match the experimental fits.

RESULTS

For nearly all vibrational modes in the condensed phase, the diagonal anharmonic shifts are smaller or comparable to the line widths. As a result, the 0 → 1 (negative intensity) and 1 → 2 (positive intensity) peaks in a 2D IR spectrum will partially overlap and destructively interfere, causing the frequency separation between the 0 → 1 and 1 → 2 peaks to appear

DOI: 10.1021/acs.jpcb.7b00537
J. Phys. Chem. B 2017, 121, 2331−2338

larger than the true anharmonic shifts (Figure S2, Table S2).[35] As such, we extract the true anharmonic shifts through a two-step process of fitting the 2D IR spectra. First, we fit slices through the 2D IR spectra taken through the peak maxima and parallel to the ω_{probe} axis using a phenomenological fit to the data in order to extract the anharmonic shift. Second, those fits are checked for accuracy by simulating the entire 2D IR spectrum with a rigorously correct formalism for the 2D line shapes. Details of the methods are presented in the Materials and Methods section and in the Supporting Information.

Because the fits to the pump slices are computationally simple, they can be quickly iterated for all of the compounds to ascertain errors. 2D IR spectra take much longer to simulate, and therefore, it is much more cumbersome to iteratively fit so many compounds. Instead, we checked that the anharmonic shifts measured from the pump slices are consistent with the full 2D IR spectra by simulating the complete 2D IR spectra for the determined anharmonic shifts. Shown in Figure 3A are the experimental 2D spectra of acetophenone in hexanes, DMSO, and D_2O. Analogous to the linear IR spectra presented in Figure 1A, the peak position shifts to lower frequencies and the line shapes become broader across the solvatochromic series. Additional experimental 2D spectra of methyl benzoate and ethyl thioacetate are shown in Figures S3A and S4A. Furthermore, determination of the CLS from the 2D IR spectra can be used to infer the frequency−frequency (or field−field[45,46]) correlation function (FFCF).[36−38] The CLS increases in a solvent-dependent manner from hexanes to D_2O (Figure 3A,B, red lines), suggesting increasing inhomogeneous broadening contributions to the line shapes.[36−39] Analysis and comparison to the simulated 2D spectra are presented below.

The experimental pump slices and phenomenological fits are shown in Figure 4 for acetophenone, where a solvent-independent anharmonic shift of 17.2 cm^{-1} (99% CI [16.9, 17.5]) was observed. Allowing the anharmonicity to be solvent-dependent produces anharmonic shifts of 17.2 cm^{-1} (99% CI [16.9, 17.5]) and 17.8 cm^{-1} (99% CI [16.2, 19.4]) for hexanes and DMSO, indicating very close agreement regardless of the anharmonicity's solvent dependence. In the case of D_2O, the greater inhomogeneous line width yields fit parameters exhibiting mutual dependency, which suggests that the equation used in the fitting is overparameterized and the anharmonic shift of 8.1 cm^{-1} (99% CI [3.8, 12.4]) is likely unphysical. Similar phenomenological fitting with methyl benzoate (Figure S5A) and ethyl thioacetate (Figure S5B) shows that the data can be well fit using constant anharmonic shifts of 17.0 cm^{-1} (99% CI [16.7, 17.2]) and 16.2 cm^{-1} (99% CI [15.5, 16.8]), respectively. Additionally, the anharmonic shifts ($\Delta = 2\omega_0\chi_e$) from 2D IR are in good agreement with overtone measurements of acetophenone, methyl benzoate, and ethyl thioacetate in hexanes and CD_3OD from linear IR measurements, in support of a solvent-independent anharmonicity (Figure S6, Table S4).

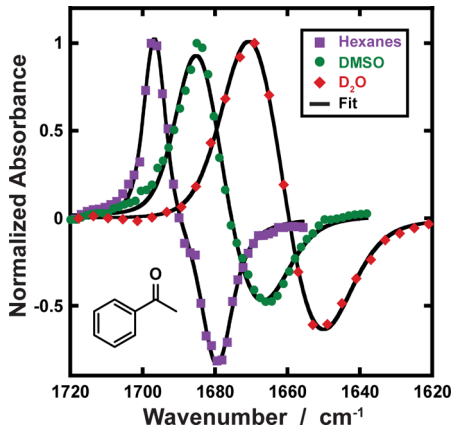

Figure 4. Acetophenone 2D solvatochromic shifts fit using a constant anharmonicity. Experimental pump slices (purple squares = hexanes; green circles = DMSO; and red diamonds = D_2O) as taken from the data presented in Figure 3 in comparison to the least-squares fitting with a constant anharmonicity (solid line). Data were collected with gratings of 150, 150, and 75 gr/mm for hexanes, DMSO, and D_2O, respectively. Comparison with fits using the lower-resolution grating (75 gr/mm) are shown in Figure S1. The anharmonic shift is determined to be 17.2 cm^{-1} (99% CI [16.9, 17.5]).

The full 2D computed spectra are shown in Figure 3B, using the anharmonic shift determined from the phenomenological fits, consistent with experiment (Figure 3A). Likewise, we observe close agreement between the overlaid pump slices from experiment and the simulated spectra (Figure 3C). The close agreement between the experimental and computed spectra in terms of the fwhm, CLS, and overall fits to the pump slice provide further evidence for a solvent-independent anharmonic shift. For methyl benzoate (Figure S3B,C) and ethyl thioacetate (Figure S4B,C), good agreement is also observed between the simulated and experimental spectra, consistent with a solvent-independent anharmonicity. Because they are not the focus of this article, the parameters used to simulate the 2D spectrum are given in Table S3. Differences in the parameters for the correlation function and the homo- and inhomogeneous line widths used to fit the pump slices are irrelevant for extracting the anharmonic shift.

The combined analysis of 2D IR data and simulated spectra suggests a solvent-independent anharmonic shift of 17.2 cm^{-1} (99% CI [16.9, 17.5]) or an anharmonicity (χ_e) of 0.00503 (99% CI [0.00495, 0.00510]) for acetophenone. Similar analysis with methyl benzoate and ethyl thioacetate also shows solvent-independent anharmonic shifts of 17.0 cm^{-1} (99% CI [16.7, 17.2]) and 16.2 cm^{-1} (99% CI [15.5, 16.8]) or anharmonicities (χ_e) of 0.00484 (99% CI [0.00478, 0.00491]) and 0.00471 (99% CI [0.00453, 0.00489]), respectively.

DISCUSSION

While the 2D IR data and analysis are consistent with a minimal effect of the solvent electric field on the carbonyl stretch anharmonicity, it is useful to turn the question around and ask how large the anharmonicity change would need to be to account for the solvent shift observed in linear IR measurements, for example, with acetophenone, where there is a frequency shift from 1696.4 cm^{-1} in hexanes to 1669.1 cm^{-1} in D_2O (Figure 1A, a difference of ~27 cm^{-1}). In other words, what change in the anharmonicity, and thus the force constant (Figure 2B), would be required to recapitulate these frequency shifts? Using the Morse potential (eq 6) and the anharmonic shift of 17.2 cm^{-1} (χ_e = 0.005) observed for acetophenone in hexanes, which for nonpolarizable MD simulations is the zero-field reference frequency, this corresponds to a harmonic frequency of ω_0 = 1713.5 cm^{-1}. Assuming that the harmonic frequency is a solvent-independent parameter and then taking the derivative of eq 7 with respect to χ_e, we would expect to observe a value of χ_e = 0.013 or an anharmonic shift (Δ_{01}) of 44.4 cm^{-1} in D_2O. This possibility is inconsistent with the 2D IR spectrum of acetophenone in D_2O as the observed peak

DOI: 10.1021/acs.jpcb.7b00537
J. Phys. Chem. B 2017, 121, 2331−2338

separation of ~20 cm^{-1} between the peak maximum/minimum of the pump slice (no fitting) sets an upper bound to the anharmonic shift.[35]

The observed constant anharmonicity indicates that the solvent's reaction field perturbs the vibrational energy levels in accordance with the linear VSE, as depicted in Figure 2A. This is in contrast to the notion of bond distortion or polarization (Figure 2B) where the vibrational potential energy surface is altered due to changes in the atomic charges, the bond length, and the force constant. Primarily, on the basis of eq 2, the harmonic frequency is obtained from the gas-phase frequency and the experimentally measured anharmonicity, and all solvent effects upon the potential will thus be observed in the frequency shifts as determined by the Stark tuning rate, consistent with other theoretical treatment of vibrational frequency shifts.[15,47−50] More rigorous treatments of the vibrational Hamiltonian and solvent dependence are also consistent with this assumption, where the dominant contribution to the environmentally induced frequency shift arises from the mechanical anharmonicity rather than the electrical anharmonicity.[3,13,24,51−54]

It is worth mentioning that these measurements and conclusions with carbonyls are not necessarily applicable to other vibrational modes including but not limited to O−H,[55−57] N−H,[58] H−Cl,[59] and coupled/delocalized amide I modes,[32,60] where the anharmonicity has been suggested to be environment-dependent. A recent study by van Wilderen et al. also showed that MeSCN exhibits a solvent-independent anharmonicity,[61] though the connection with bond polarization was not made. While the anharmonicity may be constant for carbonyls in solvents such as hexanes, DMSO, and D_2O, there is always some contribution from nonlinear and higher-order Stark effects to vibrational frequency shifts, though their contribution may be small.[9] Furthermore, while the constancy of the carbonyl bond anharmonicity, mostly in the context of the amide I band,[32,62] has been widely assumed by the 2D IR community,[43,60] these measurements provide an explicit test of these assumptions and strengthen the connection between the 2D IR and VSE perspectives. Given electric fields of sufficiently large magnitudes, that is, significantly greater than the average field in water, the bond will eventually become polarized.[9,19]

These 2D IR measurements with carbonyl vibrational probes suggests that the anharmonicity is an intrinsic property, constant across both H-bonding and non-H-bonding solvents. These findings are in agreement with the limited prior literature from overtone experiments in diverse solvents as well as in the gas phase.[30,58,63,64] This expands upon prior work, which has characterized the Stark tuning rate of various carbonyl probes, finding that the Stark tuning rate is constant across multiple solvents both with and without H-bonding, allowing for quantitative mapping of electric fields from observed vibrational frequencies.[7,8] That is, solvents exerting different electric fields do not perturb the bond's force constant or atomic charges, as described by bond polarization models, but rather modify the corresponding energy levels according to the VSE. This has important ramifications for interpretation and rationalization of carbonyl frequency shifts in the condensed phase. It will be very interesting to extend these measurements to carbonyl probes at the active sites of enzymes where even larger frequency shifts to the red, interpreted as still larger electric fields than those in solution, are present.[8,9,16]

CONCLUSIONS

Though intrinsic or added vibrational probes have long been recognized as a method for ascertaining local information about noncovalent interactions in complex environments, the physical origins of vibrational frequency shifts continue to be debated. Among the prevailing interpretations of observed frequency shifts is bond polarization,[21−23] whereby the bond force constant is perturbed and is often discussed in terms of the stabilizing effect of more polar solvents on resonance structures with weaker bonds. However, in the case of carbonyls (and nitriles), an alternative body of research, based largely on simulations, suggests that the observed vibrational solvatochromism can be explained primarily in terms of the linear VSE whereby the environment's electric field alters the vibrational energy levels based on the probe's intrinsic Stark tuning rate.[4,7,8] This model assumes that the Stark tuning rate is constant across diverse environments such as in the presence and absence of hydrogen bonding, and this is consistent with vibrational Stark spectroscopy data and MD simulations.[7−9,19,20]

These two models for vibrational frequency shifts would be expected to exhibit different trends in their bond anharmonicity across different solvents, which can be tested by measuring the anharmonic shifts using overtone absorption or 2D IR. Using 2D IR spectroscopy, the anharmonic shifts were found to be constant within experimental error across hexanes, DMSO, and D_2O for the carbonyl groups of acetophenone, methyl benzoate, and ethyl thioacetate based on fits to the pump slices. The accuracy of these fits was compared against simulated 2D IR spectra using a rigorously correct formalism for the 2D line shapes, finding good agreement with experiment. Together, these findings suggest that the solvatochromic response of carbonyl vibrational probes is better described by the VSE than bond polarization mechanisms. For carbonyls, these findings provide a clear physical interpretation for solvatochromic frequency shifts, supporting the linear VSE (and a variety of solvent simulations). This can then be used as a calibration to extract quantitative information on the electric field experienced by the probe in complex environments, such as enzyme active sites, for the study of noncovalent interactions.

ASSOCIATED CONTENT

Supporting Information

The Supporting Information is available free of charge on the ACS Publications website at DOI: 10.1021/acs.jpcb.7b00537.

Additional methods for FTIR overtone measurements, relationship between the apparent anharmonic shift and line width, grating dependence on experimental fits, experimental and simulated methyl benzoate and ethyl thioacetate spectra, FTIR overtone spectra, apparent anharmonic shifts, comparison of linear and 2D IR fundamental frequencies, simulated and experimental 2D IR line shape parameters, and FTIR overtone peak positions (PDF)

AUTHOR INFORMATION

ORCID

Samuel H. Schneider: 0000-0002-5792-4015
Huong T. Kratochvil: 0000-0001-8039-6823
Martin T. Zanni: 0000-0001-7191-9768

DOI: 10.1021/acs.jpcb.7b00537
J. Phys. Chem. B 2017, 121, 2331−2338

Present Address

[⊥]H.T.K.: Department of Pharmaceutical Chemistry, University of California—San Francisco, San Francisco, California 91458, USA.

Notes

The authors declare no competing financial interest.

■ ACKNOWLEDGMENTS

We would like to thank the Stanford Department of Statistics Consulting Services for assistance with modeling and statistical analysis. This work was supported in part by grants from the NIH (Grant GM27738 and GM118044 to S.G.B. and DK079895 and GM102387 to M.T.Z.).

■ REFERENCES

(1) Liptay, W. Electrochromism and Solvatochromism. *Angew. Chem., Int. Ed. Engl.* **1969**, *8*, 177−188.

(2) Marini, A.; Munoz-Losa, A.; Biancardi, A.; Mennucci, B. What is Solvatochromism? *J. Phys. Chem. B* **2010**, *114*, 17128−17135.

(3) Cho, M. Vibrational Solvatochromism and Electrochromism: Coarse-Grained Models and Their Relationships. *J. Chem. Phys.* **2009**, *130*, 094505.

(4) Choi, J.-H.; Cho, M. Vibrational Solvatochromism and Electrochromism of Infrared Probe Molecules Containing C≡O, C≡N, C═O, or C-F Vibrational Chromophore. *J. Chem. Phys.* **2011**, *134*, 154513.

(5) Badger, R. M.; Bauer, S. H. Spectroscopic Studies of the Hydrogen Bond. II. The Shift of the O−H Vibrational Frequency in the Formation of the Hydrogen Bond. *J. Chem. Phys.* **1937**, *5*, 839−851.

(6) Fried, S. D.; Boxer, S. G. Measuring Electric Fields and Noncovalent Interactions Using the Vibrational Stark Effect. *Acc. Chem. Res.* **2015**, *48*, 998−1006.

(7) Fried, S. D.; Bagchi, S.; Boxer, S. G. Measuring Electrostatic Fields in Both Hydrogen-Bonding and Non-Hydrogen-Bonding Environments Using Carbonyl Vibrational Probes. *J. Am. Chem. Soc.* **2013**, *135*, 11181−11192.

(8) Schneider, S. H.; Boxer, S. G. Vibrational Stark Effects of Carbonyl Probes Applied to Re-interpret IR and Raman Data for Enzyme Inhibitors in Terms of Electric Fields at the Active Site. *J. Phys. Chem. B* **2016**, *120*, 9672−9684.

(9) Fried, S. D.; Bagchi, S.; Boxer, S. G. Extreme Electric Fields Power Catalysis in the Active Site of Ketosteroid Isomerase. *Science* **2014**, *346*, 1510−1514.

(10) Edington, S. C.; Flanagan, J. C.; Baiz, C. R. An Empirical IR Frequency Map for Ester C═O Stretching Vibrations. *J. Phys. Chem. A* **2016**, *120*, 3888−96.

(11) Fried, S. D.; Wang, L. P.; Boxer, S. G.; Ren, P.; Pande, V. S. Calculations of the Electric Fields in Liquid Solutions. *J. Phys. Chem. B* **2013**, *117*, 16236−16248.

(12) In vibrational Stark spectroscopy (VSS), the applied external electric field, $\vec{F}_{ext}$, is known precisely from the sample thickness and applied voltage, while the local field experienced by the probe is modified according to, $\vec{F}_{local} = f\vec{F}_{ext}$, where f is the local field factor, a tensor, though generally treated as a scalar. As the value of the local field factor is uncertain, the measured Stark tuning rate from VSS is reported as $|\Delta\vec{\mu}_{probe}|f$. In contrast, there is no applied electric field for the vibrational solvatochromism and MD simulations. This leads to a difference in the Stark tuning rate as determined by VSS relative to the slope of the field−frequency correlation ($|\Delta\vec{\mu}_{probe}|$), where the difference is assumed to be a measure of the local field factor, such that $f \approx 2$. This is discussed in depth in refs 6−9, as well as Böttcher, C. J. F.; van Belle, O. C.; Bordewijk, P.; Rip, A. *Theory of Electric Polarization*, 2nd ed.; Elsevier Publishing Co.: Amsterdam, The Netherlands, 1973; Vol. *1*.

(13) Błasiak, B.; Cho, M. Vibrational Solvatochromism. II. A First-Principle Theory of Solvation-Induced Vibrational Frequency Shift Based on Effective Fragment Potential Method. *J. Chem. Phys.* **2014**, *140*, 164107.

(14) Błasiak, B.; Cho, M. Vibrational Solvatochromism. III. Rigorous Treatment of the Dispersion Interaction Contribution. *J. Chem. Phys.* **2015**, *143*, 164111.

(15) Schmidt, J. R.; Corcelli, S. A.; Skinner, J. L. Ultrafast Vibrational Spectroscopy of Water and Aqueous *N*-Methylacetamide: Comparison of Different Electronic Structure/Molecular Dynamics Approaches. *J. Chem. Phys.* **2004**, *121*, 8887−8896.

(16) Wu, Y.; Boxer, S. G. A Critical Test of the Electrostatic Contribution to Catalysis with Noncanonical Amino Acids in Ketosteroid Isomerase. *J. Am. Chem. Soc.* **2016**, *138*, 11890−11895.

(17) Morse, P. M. Diatomic Molecules According to the Wave Mechanics. II. Vibrational Levels. *Phys. Rev.* **1929**, *34*, 57−64.

(18) Atkins, P.; De Paula, J. *Physical Chemistry*, 10th ed.; Oxford University Press: Oxford, U.K., 2014.

(19) Dalosto, S. D.; Vanderkooi, J. M.; Sharp, K. A. Vibrational Stark Effects on Carbonyl, Nitrile, and Nitrosyl Compounds Including Heme Ligands, CO, CN, and NO, Studied with Density Functional Theory. *J. Phys. Chem. B* **2004**, *108*, 6450−6457.

(20) List, N. H.; Beerepoot, M. T.; Olsen, J. M.; Gao, B.; Ruud, K.; Jensen, H. J.; Kongsted, J. Molecular Quantum Mechanical Gradients Within the Polarizable Embedding Approach—Application to the Internal Vibrational Stark Shift of Acetophenone. *J. Chem. Phys.* **2015**, *142*, 034119.

(21) Anderson, V. E. Quantifying Energetic Contributions to Ground State Destabilization. *Arch. Biochem. Biophys.* **2005**, *433*, 27−33.

(22) Carey, P. R. Spectroscopic Characterization of Distortion in Enzyme Complexes. *Chem. Rev.* **2006**, *106*, 3043−3054.

(23) Kurz, L. C.; Drysdale, G. R. Evidence from Fourier Transform Infrared Spectroscopy for Polarization of the Carbonyl of Oxaloacetate in the Active Site of Citrate Synthase. *Biochemistry* **1987**, *26*, 2623−2627.

(24) Torii, H. Amide I Vibrational Properties Affected by Hydrogen Bonding Out-of-Plane of the Peptide Group. *J. Phys. Chem. Lett.* **2015**, *6*, 727−733.

(25) McDowell, S. A. C.; Buckingham, A. D. On the Correlation Between Bond-Length Change and Vibrational Frequency Shift in Hydrogen-Bonded Complexes: A Computational Study of Y···HCl Dimers (Y = N_2, CO, BF). *J. Am. Chem. Soc.* **2005**, *127*, 15515−15520.

(26) Hush, N. S.; Williams, M. L. Carbon Monoxide Bond Length, Force Constant and Infrared Intensity Variations in Strong Electric Fields: Valence-Shell Calculations, with Applications to Properties of Adsorbed and Complexed CO. *J. Mol. Spectrosc.* **1974**, *50*, 349−368.

(27) Park, E. S.; Boxer, S. G. Origins of the Sensitivity of Molecular Vibrations to Electric Fields: Carbonyl and Nitrosyl Stretches in Model Compounds and Proteins. *J. Phys. Chem. B* **2002**, *106*, 5800−5806.

(28) Andrews, S. S.; Boxer, S. G. Vibrational Stark Effects of Nitriles I. Methods and Experimental Results. *J. Phys. Chem. A* **2000**, *104*, 11853−11863.

(29) Park, E. S.; Andrews, S. S.; Hu, R. B.; Boxer, S. G. Vibrational Stark Spectroscopy in Proteins: A Probe and Calibration for Electrostatic Fields. *J. Phys. Chem. B* **1999**, *103*, 9813−9817.

(30) Chen, Y.; Morisawa, Y.; Futami, Y.; Czarnecki, M. A.; Wang, H.-S.; Ozaki, Y. Combined IR/NIR and Density Functional Theory Calculations Analysis of the Solvent Effects on Frequencies and Intensities of the Fundamental and Overtones of the C═O Stretching Vibrations of Acetone and 2-Hexanone. *J. Phys. Chem. A* **2014**, *118*, 2576−2583.

(31) DeFlores, L. P.; Ganim, Z.; Ackley, S. F.; Chung, H. S.; Tokmakoff, A. The Anharmonic Vibrational Potential and Relaxation Pathways of the Amide I and II Modes of *N*-Methylacetamide. *J. Phys. Chem. B* **2006**, *110*, 18973−18980.

(32) Wang, J.; Hochstrasser, R. M. Anharmonicity of Amide Modes. *J. Phys. Chem. B* **2006**, *110*, 3798−3807.

(33) Shim, S. H.; Zanni, M. T. How to Turn Your Pump-Probe Instrument into a Multidimensional Spectrometer: 2D IR and Vis

DOI: 10.1021/acs.jpcb.7b00537
J. Phys. Chem. B 2017, 121, 2331−2338

Spectroscopies via Pulse Shaping. *Phys. Chem. Chem. Phys.* **2009**, *11*, 748−761.
(34) Ghosh, A.; Serrano, A. L.; Oudenhoven, T. A.; Ostrander, J. S.; Eklund, E. C.; Blair, A. F.; Zanni, M. T. Experimental Implementations of 2D IR Spectroscopy Through a Horizontal Pulse Shaper Design and a Focal Plane Array Detector. *Opt. Lett.* **2016**, *41*, 524−527.
(35) Hamm, P.; Zanni, M. *Concepts and Methods of 2D Infrared Spectroscopy*, 1st ed.; Cambridge University Press: Cambridge, U.K., 2011.
(36) Fenn, E. E.; Fayer, M. D. Extracting 2D IR Frequency-Frequency Correlation Functions from Two Component Systems. *J. Chem. Phys.* **2011**, *135*, 074502.
(37) Kwak, K.; Park, S.; Finkelstein, I. J.; Fayer, M. D. Frequency-Frequency Correlation Functions and Apodization in Two-Dimensional Infrared Vibrational Echo Spectroscopy: A New Approach. *J. Chem. Phys.* **2007**, *127*, 124503.
(38) Park, S.; Fayer, M. D. Hydrogen Bond Dynamics in Aqueous NaBr Solutions. *Proc. Natl. Acad. Sci. U. S. A.* **2007**, *104*, 16731−8.
(39) Kwak, K.; Rosenfeld, D. E.; Fayer, M. D. Taking Apart the Two-Dimensional Infrared Vibrational Echo Spectra: More Information and Elimination of Distortions. *J. Chem. Phys.* **2008**, *128*, 204505.
(40) Mukamel, S. *Principles of Nonlinear Optical Spectroscopy*; Oxford University Press: New York, 1995.
(41) Wang, L.; Middleton, C. T.; Zanni, M. T.; Skinner, J. L. Development and Validation of Transferable Amide I Vibrational Frequency Maps for Peptides. *J. Phys. Chem. B* **2011**, *115*, 3713−3724.
(42) Kashid, S. M.; Jin, G. Y.; Bagchi, S.; Kim, Y. S. Cosolvent Effects on Solute-Solvent Hydrogen-Bond Dynamics: Ultrafast 2D IR Investigations. *J. Phys. Chem. B* **2015**, *119*, 15334−15343.
(43) DeCamp, M. F.; DeFlores, L.; McCracken, J. M.; Tokmakoff, A.; Kwac, K.; Cho, M. Amide I Vibrational Dynamics of *N*-Methylacetamide in Polar Solvents: The Role of Electrostatic Interactions. *J. Phys. Chem. B* **2005**, *109*, 11016−11026.
(44) Hamm, P.; Lim, M.; Hochstrasser, R. M. Structure of the Amide I Band of Peptides Measured by Femtosecond Nonlinear-Infrared Spectroscopy. *J. Phys. Chem. B* **1998**, *102*, 6123−6138.
(45) Eaves, J. D.; Tokmakoff, A.; Geissler, P. A. Electric Field Fluctuations Drive Vibrational Dephasing in Water. *J. Phys. Chem. A* **2005**, *109*, 9424−9436.
(46) Corcelli, S. A.; Lawrence, C. P.; Skinner, J. L. Combined Electronic Structure/Molecular Dynamics Approach for Ultrafast Infrared Spectroscopy of Dilute HOD in Liquid H_2O and D_2O. *J. Chem. Phys.* **2004**, *120*, 8107−8117.
(47) Malolepsza, E.; Straub, J. E. Empirical Maps for the Calculation of Amide I Vibrational Spectra of Proteins from Classical Molecular Dynamics Simulations. *J. Phys. Chem. B* **2014**, *118*, 7848−7855.
(48) Ham, S.; Kim, J.-H.; Lee, H.; Cho, M. Correlation Between Electronic and Molecular Structure Distortions and Vibrational Properties. II. Amide I modes of NMA−$n$$D_2O$ Complexes. *J. Chem. Phys.* **2003**, *118*, 3491−3498.
(49) Hayashi, T.; Hamaguchi, H.-o. Solvent Induced Dynamic Polarization, Vibrational Dephasing, and Infrared Band Shape of the C═O Stretch Mode of Acetone in Acetonitrile: A New Theoretical Approach. *Chem. Phys. Lett.* **2000**, *326*, 115−122.
(50) Reppert, M.; Tokmakoff, A. Electrostatic Frequency Shifts in Amide I Vibrational Spectra: Direct Parameterization Against Experiment. *J. Chem. Phys.* **2013**, *138*, 134116.
(51) Hush, N. S.; Reimers, J. R. Vibrational Stark Spectroscopy. 1. Basic Theory and Application to the CO Stretch. *J. Phys. Chem.* **1995**, *99*, 15798−15805.
(52) Błasiak, B.; Lee, H.; Cho, M. Vibrational Solvatochromism: Towards Systematic Approach to Modeling Solvation Phenomena. *J. Chem. Phys.* **2013**, *139*, 044111.
(53) Torii, H. Vibrational Interactions in the Amide I Subspace of the Oligomers and Hydration Clusters of *N*-Methylacetamide. *J. Phys. Chem. A* **2004**, *108*, 7272−7280.
(54) Torii, H. Electrostatic Origin of the Cooperative Effect on the C═O Bond Lengths and the Amide I Vibrational Frequencies of the *N*-Methylacetamide Oligomers. *J. Mol. Struct.* **2005**, *735*−*736*, 21−26.
(55) Keinan, S.; Pines, D.; Kiefer, P. M.; Hynes, J. T.; Pines, E. Solvent-Induced O-H Vibration Red-Shifts of Oxygen-Acids in Hydrogen-Bonded O-H···Base Complexes. *J. Phys. Chem. B* **2015**, *119*, 679−692.
(56) Kiefer, P. M.; Pines, E.; Pines, D.; Hynes, J. T. Solvent-Induced Red-Shifts for the Proton Stretch Vibrational Frequency in a Hydrogen-Bonded Complex. 1. A Valence Bond-Based Theoretical Approach. *J. Phys. Chem. B* **2014**, *118*, 8330−8351.
(57) Péron, J. J.; Sandorfy, C. The Anharmonicity of the OH Stretching Vibration of Hydrogen Bonded Methanol in Binary Systems. *J. Chem. Phys.* **1976**, *65*, 3153−3157.
(58) Foldes, A.; Sandorfy, C. Anharmonicity and Hydrogen Bonding Part III. Examples of Strong Bonds. General Discussion. *J. Mol. Spectrosc.* **1966**, *20*, 262−275.
(59) Perrot, M.; Turrell, G.; Huong, P. V. Vibrational Anharmonicity of HCl in Solution. *J. Mol. Spectrosc.* **1970**, *34*, 47−52.
(60) Reppert, M.; Tokmakoff, A. Computational Amide I 2D IR Spectroscopy as a Probe of Protein Structure and Dynamics. *Annu. Rev. Phys. Chem.* **2016**, *67*, 359−386.
(61) van Wilderen, L. J.; Kern-Michler, D.; Muller-Werkmeister, H. M.; Bredenbeck, J. Vibrational Dynamics and Solvatochromism of the Label SCN in Various Solvents and Hemoglobin by Time Dependent IR and 2D-IR Spectroscopy. *Phys. Chem. Chem. Phys.* **2014**, *16*, 19643−19653.
(62) Wang, J.; Zhuang, W.; Mukamel, S.; Hochstrasser, R. M. Two-Dimensional Infrared Spectroscopy as a Probe of the Solvent Electrostatic Field for a Twelve Residue Peptide. *J. Phys. Chem. B* **2008**, *112*, 5930−5937.
(63) la Cour Jansen, T.; Knoester, J. A Transferable Electrostatic Map for Solvation Effects on Amide I Vibrations and its Application to Linear and Two-Dimensional Spectroscopy. *J. Chem. Phys.* **2006**, *124*, 044502.
(64) Bayliss, N. S.; Cole, A. R. H.; Little, L. H. Solvent Effects in Infra-Red Spectra: C═O, C-H, and C-C Vibrations. *Aust. J. Chem.* **1955**, *8*, 26−38.

DOI: 10.1021/acs.jpcb.7b00537
J. Phys. Chem. B 2017, 121, 2331−2338

Supplementary Information for

Solvent-Independent Anharmonicity for Carbonyl Oscillators

Samuel H. Schneider,[a] Huong T. Kratochvil,[b,c] Martin T. Zanni,[b] * Steven G. Boxer[a] *

[a] Department of Chemistry, Stanford University, Stanford, California, 94305-5012, USA
[b] Department of Chemistry, University of Wisconsin-Madison, Madison, Wisconsin, 53706, USA
[c] Current address: Department of Pharmaceutical Chemistry, University of California-San Francisco, San Francisco, California, 91458, UA

* Corresponding authors

Table of Contents:

1. Additional Methods:

FTIR Overtone Measurements:

FTIR spectra were recorded on a Bruker Vertex 70 spectrometer with a liquid nitrogen-cooled mercury cadmium telluride (MCT) detector using methods described previously.[1] Briefly, a demountable liquid cell was prepared from two CaF_2 optical windows (0.75 in diameter, 0.25 in thickness, Red Optronics), separated by two Teflon spacers (75 and 100 μm thickness), to which 20-30 μL of 200 mM solute solution was added. High concentrations of solute are required to observe the carbonyl overtones due to the roughly two-orders of magnitude lower intensity of the first overtone relative to the fundamental transition.[2]

Transmission spectra were acquired by averaging 256 scans after 10 mins of purging with a nitrogen flow to remove atmospheric CO_2 and water vapor. Spectra were recorded from 4000-1400 cm^{-1} with 1 cm^{-1} resolution and aperture settings from 2-6 mm in order to maximize signal intensity. The absorption spectra were calculated by taking the negative logarithm of the difference between solute and neat solvent transmission spectra. All solvatochromism measurements were repeated in triplicate, and all frequencies determined using the OPUS software's peak picker (Bruker) as well as pseudo-Voigt fitting with the Levenberg-Marquardt algorithm.

2. Supplementary Figures:

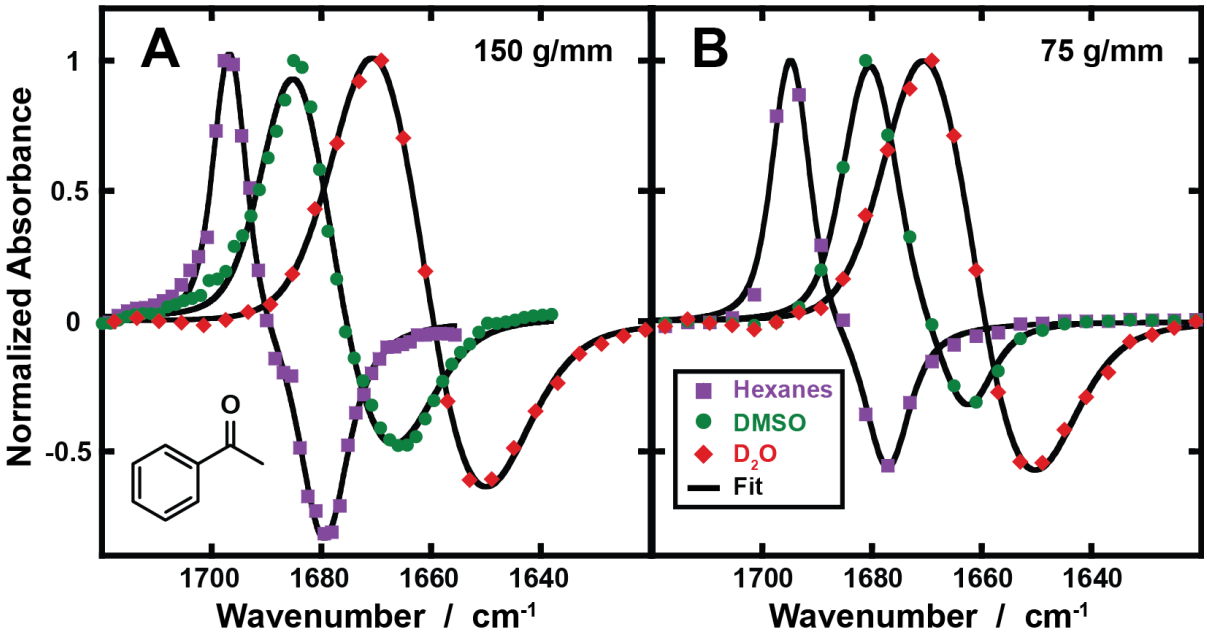

Figure S1. Anharmonicity solvent-dependence is independent of grating. Normalized experimental pump slices from 2D IR spectra taken with either a (A) 150 or (B) 75 g/mm grating and the pump slices fit using the method described in the main text with a constant anharmonicity. Experimental data is shown (purple squares = hexanes, green circles = DMSO, and red diamond = D_2O) with fits shown with solid black lines. The anharmonic shift is determined to be 17.2 cm^{-1} 99% CI [16.9, 17.5] and 17.6 cm^{-1} 99% CI [17.3, 17.9] for the 150 and 75 g/mm gratings respectively, indicating that these values are not significantly different at the 99% CI.

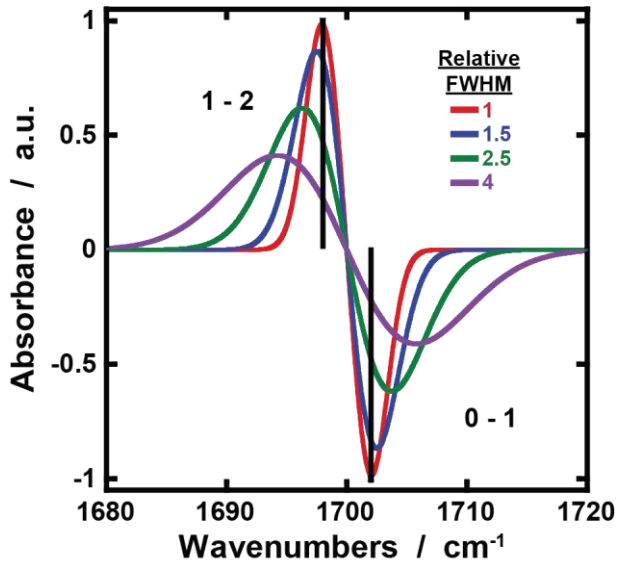

Figure S2. Change in the apparent anharmonic shift as a function of FWHM. Given a constant fixed frequency (black vertical lines) and anharmonicity of the 0-1 (negative) and 1-2 (positive) transitions, demonstrated here using guassians of an intensity of 1, the apparent anharmonic shift increases as the relative FWHM of the peaks increases (see Table S1).[3] Determining the true anharmonic shift requires more complex fitting of the data.

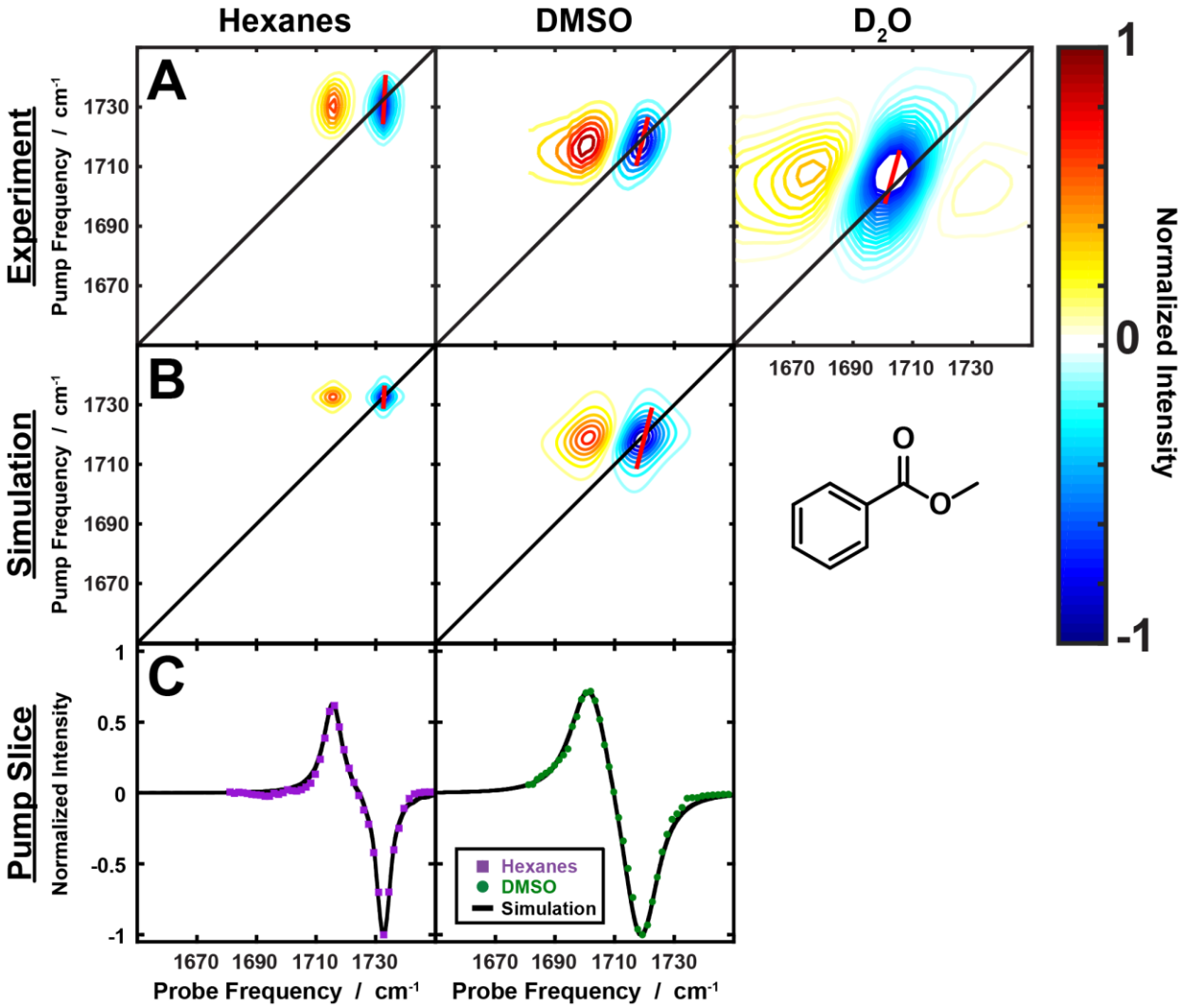

Figure S3. Experimental and simulated 2D IR spectra of methyl benzoate in hexanes, DMSO, and D_2O. (Row A) Experimental 2D IR spectra and (Row B) simulated spectra using fixed anharmonicity and population relaxation (T_1). The fundamental (blue) and 1 → 2 (red) transition are shown for each spectra, with center line slopes shown in red. Details on the CLS fitting and 2D simulated spectra are described in the methods section. (Row C) Overlay of the pump slices from experiment (purple squares, green circles) and best fit from simulation (black solid line) along the peak maximum for different solvents. Experimental and simulated lineshape parameters are reported in Table S3. In D_2O, there is an additional off-diagonal peak at ca. 1730 cm^{-1} that partially cancels the intensity of the fundamental, making accurate extraction of lineshape parameters and subsequent simulation difficult.

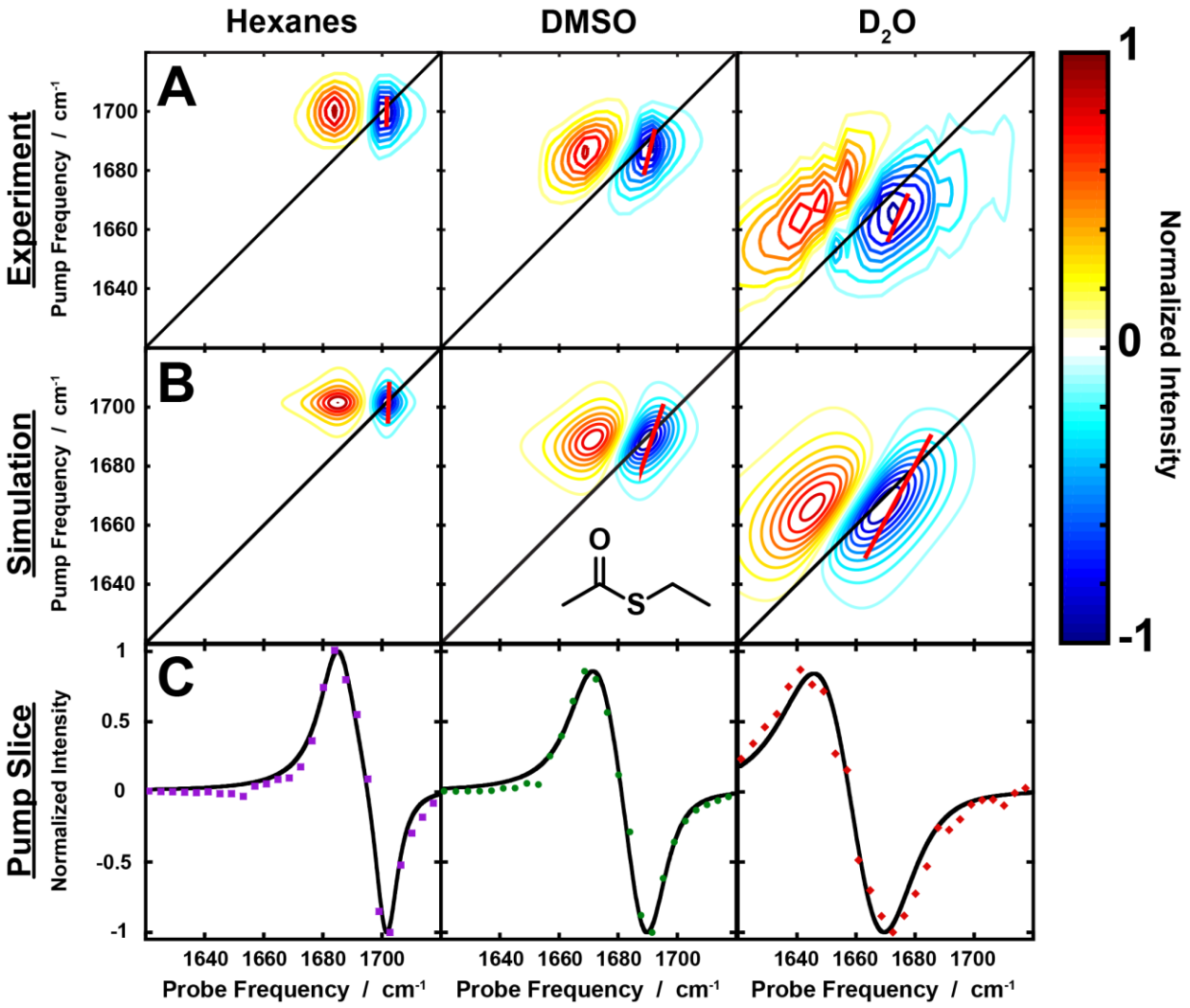

Figure S4. Experimental and simulated 2D IR spectra of ethyl thioacetate in hexanes, DMSO, and D_2O. (Row A) Experimental 2D IR spectra and (Row B) simulated spectra using fixed anharmonicity and population relaxation (T_1). The fundamental (blue) and $1 \rightarrow 2$ (red) transition are shown for each spectra, with center line slopes shown in red. Details on the CLS fitting and 2D simulated spectra are described in the methods section. (Row C) Overlay of the pump slices from experiment (purple, green) and best fit from simulation (black) along the peak maximum for different solvents. Experimental and simulated lineshape parameters are reported in Table S3. Ethyl thioacetate is not very soluble in D_2O, thus decreasing the signal-to-noise which influences the extraction of accurate lineshape parameters.

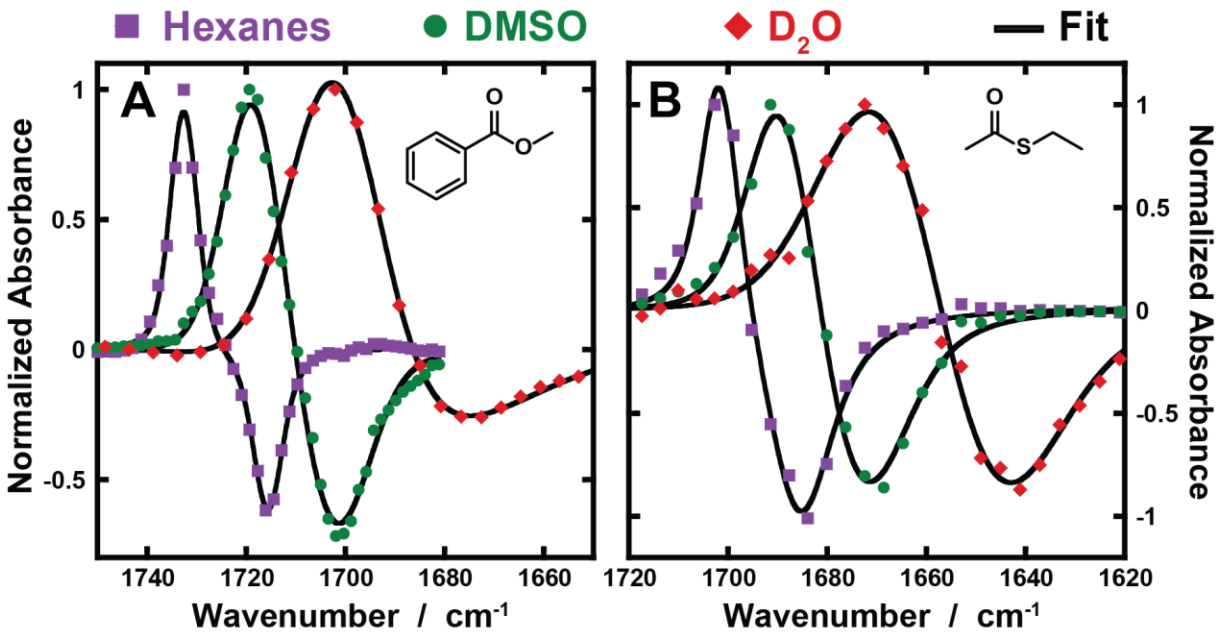

Figure S5. Solvent-independent anharmonicity for methyl benzoate and ethyl thioacetate. Normalized experimental pump slices from 2D IR spectra and fits using the method described in the main text with a constant anharmonicity. Experimental data is shown as solid colored lines (purple squares = hexanes, green circles = DMSO, and red diamonds = D_2O) while the fits are shown with solid lines. The anharmonic shift is determined to be 17.0 cm^{-1} 99% CI [16.7, 17.2] and 16.2 cm^{-1} 99% CI [15.5, 16.8] for (A) methyl benzoate and (B) ethyl thioacetate respectively.

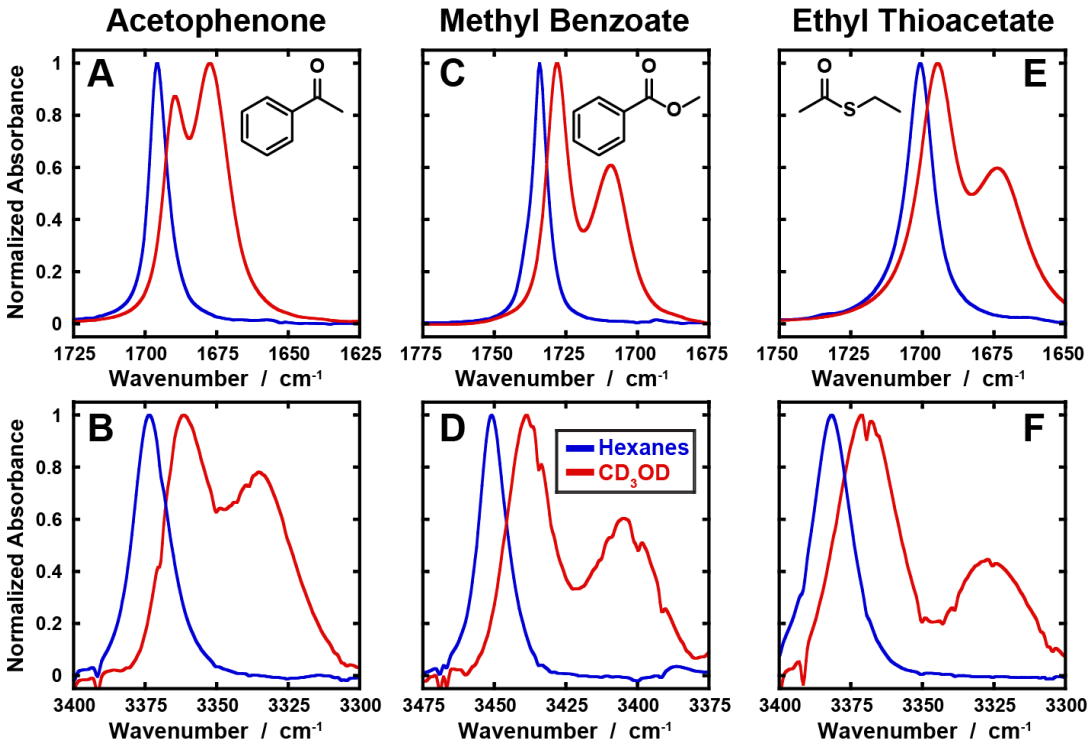

Figure S6. Carbonyl fundamental and overtone spectra in hexanes and CD_3OD. (A, C, E) Fundamental C=O stretch of 200 mM acetophenone, methyl benzoate, and ethyl thioacetate in hexanes (blue) and CD_3OD (red). (B, D, F) Overtone C=O stretch of acetophenone, methyl benzoate and ethyl thioacetate. The two peaks observed for all solutes in CD_3OD corresponds to 0- and 1-H-bonding configurations.

3. Supplemental Tables:

Table S1. Comparison between linear and 2D IR frequencies and FWHM for the fundamental transition of acetophenone.

Solvent	**Linear IR** [a] $\bar{\nu}_{01}$ **(cm^{-1})**	**Linear IR** [a] **FWHM (cm^{-1})**	**2D IR** $\bar{\nu}_{01}$ **(cm^{-1})** [c]	**2D IR FWHM (cm^{-1})** [c]
Hexanes	1696.4	6.4	1696.7 [1696.5, 1696.9] [b]	7.1 [6.5, 7.7] [b]
DMSO	1682.0	11.0	1684.8 [1684.5, 1685.2] [b]	14.3 [13.5, 15.1] [b]
D_2O	1669.4	21.4	1669.5 [1669.1, 1669.9] [b]	19.2 [17.8, 20.6] [b]

[a] Values as reported by Fried *et al*.[1]

[b] Values in brackets are the 99% confidence intervals from the pump slice fitting.

[c] While generally close to the observed frequency and FWHM compared to the linear spectrum, the pump slices were taken from those with the maximum intensity, which based on the resolution of these measurements (~3 cm^{-1}) and the CLS, could lead to a potential shift in the center frequency and FWHM from those in the linear spectrum.

Table S2. Apparent anharmonic shifts for carbonyl oscillators in hexanes, DMSO, and D_2O as determined from peak minima/maxima of the experimental pump slices.

Solute	Solvent	Grating [a] (g/mm)	$\bar{\nu}_{01}^{app}$ [b, d] (cm^{-1})	$\bar{\nu}_{12}^{app}$ [b] (cm^{-1})	Δ^{app} [c] (cm^{-1})
Acetophenone	Hexanes [Exp't]	150	1697 [1696.4±0.1]	1680	17
	Hexanes [Exp't]	75	1693 [1696.4±0.1]	1677	16
	DMSO [Exp't]	150	1685 [1681.9±0.1]	1665	20
	DMSO [Exp't]	75	1681 [1681.9±0.1]	1661	20
	D_2O [Exp't]	75	1669 [1669.1±0.3]	1649	20
Methyl Benzoate	Hexanes [Exp't]	150	1733 [1734.5±0.1]	1716	17
	Hexanes [Exp't]	75	1729 [1734.5±0.1]	1711	18
	DMSO [Exp't]	150	1719 [1719.7±0.1]	1702	17
	DMSO [Exp't]	75	1711 [1719.7±0.1]	1693	18
	D_2O [Exp't]	75	1702 [1704.0±0.5]	1674	28
Ethyl Thioacetate	Hexanes [Exp't]	150	1702 [1701.1±0.1]	1684	18
	Hexanes [Exp't]	75	1702 [1701.1±0.1]	1684	18
	DMSO [Exp't]	150	1690 [1686.0±0.2]	1669	21
	DMSO [Exp't]	75	1692 [1686.0±0.2]	1669	23
	D_2O [Exp't]	75	1669-1680 [e] [1663.0±0.4]	1641-1653 [e]	27-31

[a] The 150 and 75 gratings have different resolutions of 3 and 5 cm^{-1}, respectively, which introduces an uncertainty in the true peak positions and anharmonic shift (Δ^{app}).

[b] The reported frequencies correspond to the maxima/minima of the pump slice with maximum intensity.

[c] The apparent anharmonic shift sets an upper limit on the true anharmonic shift and will appear to increase with solvents of increasing electric field due to increased broadening and overlap in cases where the FWHM is of a similar magnitude to the anharmonic shift (see Fig S1).

[d] Experimental frequencies for the $\bar{\nu}_{01}$ from linear IR measurements, at the same concentration, are shown in brackets for comparison.[1, 4]

[e] The reported range is due to the low solubility in D_2O. The pump slices with the maximum intensity are at different frequencies which will cause a change in the peak position due to the CLS.

Table S3. Parameters used for simulating 2D IR (Figure S3 and S4) spectra with constant anharmonicity and corresponding lineshape parameters for methyl benzoate and ethyl thioacetate in hexanes, DMSO, and D_2O.[a]

Solute	Solvent	T_2^* [c] (ps)	Δ_1 (ps^{-1})	$FWHM_{01}$ (cm^{-1})	$FWHM_{12}$ (cm^{-1})	CLS [d]
Acetophenone	Hexanes	6.377	0.042	7.0	11.1	0.12
	Experiment[b]			7.1 [6.5, 7.7]	11.0 [10.0, 12.0]	0.12±0.01
	DMSO	0.617	0.405	14.3	18.2	0.33
	Experiment[b]			14.3 [13.5, 15.1]	19.0 [16.9, 21.1]	0.33±0.01
	D_2O	0.208	0.720	19.2	23.0	0.36
	Experiment[b]			19.2 [17.8, 20.7]	22.0 [19.3, 24.7]	0.36±0.01
Methyl Benzoate	Hexanes	1.435	0.005	5.7	7.7	0.05
	Experiment[b]			6.7 [6.2, 7.2]	7.4 [6.6, 8.2]	0.05±01
	DMSO	0.282	0.180	13.8	15.6	0.25
	Experiment[b]			13.8 [13.2, 14.4]	16.3 [15.2, 17.4]	0.25±0.01
	D_2O[e]					
	Experiment[b]			22.1 [21.1, 23.1]	48.0 [40.3, 55.3]	0.30±0.01
Ethyl Thioacetate	Hexanes	1.339	0.010	9.7	16.1	0.03
	Experiment[b]			9.7 [8.1, 11.3]	16.1 [15.4, 16.8]	0.03±0.01
	DMSO	0.482	0.660	16.2	21.7	0.34
	Experiment[b]			16.2 [14.5, 17.7]	23.3 [19.7, 26.9]	0.34±0.04
	D_2O	0.088	11.940	27.9	31.4	0.54
	Experiment[b]			27.9 [24.9, 30.9]	38.4 [31.5, 45.3]	0.54±0.09

[a] Spectra were simulated with a constant anharmonicity, as determined from fits to the pump slices, and a constant population relaxation time (T_1) of 1175, 2500, and 840 fs for acetophenone, methyl benzoate, and ethyl thioacetate, respectively, using a correlation function, $C(t) = \Delta_0^2 e^{-t/\tau_1} + \Delta_1^2$.

[b] Experimental 2D IR parameters as determined from global fitting of the pump slices described in the text with 99% confidence interval in brackets.

[c] The pure dephasing time (T_2^*) as defined by $\frac{1}{\Delta_0^2 \tau_0}$.

[d] Center line slopes were determined according to the CLSω_m method, see methods section for details.

[e] The 2D spectrum of methyl benzoate in D_2O was not simulated due to the presence of an additional off-diagonal peak at 1730 cm^{-1}, that prevents accurate extraction of lineshape parameters for simulating.

Table S4. FTIR overtone measurements for acetophenone, methyl benzoate, and ethyl thioacetate in hexanes and CD_3OD.

Solute	Solvent	$\bar{\nu}_{01}$ (cm^{-1})	$\bar{\nu}_{02}$ (cm^{-1})	$2\omega_0\chi_e$ (cm^{-1}) [a]
Acetophenone	Hexanes	1695.6±0.2	3373.6±0.4	17.6±0.6
	CD_3OD [b]	1689.8±0.3	3362.8±0.9	16.8±1.1
		1677.2±0.1	3337.0±0.5	17.2±0.5
Methyl Benzoate	Hexanes	1734.1±0.1	3450.9±0.2	17.3±0.3
	CD_3OD [b]	1728.1±0.1	3438.5±1.0	17.7±1.0
		1709.4±0.1	3402.0±2.0	16.8±2.0
Ethyl Thioacetate	Hexanes	1700.8±0.1	3381.8±0.2	19.8±0.3
	CD_3OD [b]	1694.8±0.2	3371.3±1.7	18.3±1.7
		1673.2±0.6	3325.6±1.9	20.8±2.2

[a] This value is multiplied by two for comparison with the anharmonic shifts as observed by 2D IR in the main text. $2\omega_0\chi_e = \Delta = 2\bar{\nu}_{01} - \bar{\nu}_{02} = \bar{\nu}_{01} - \bar{\nu}_{12}$. [b] The two frequencies reported in CD_3OD correspond to 0- and 1-H-bonding configurations.

4. References:

(1) Fried, S. D.; Bagchi, S.; Boxer, S. G. Measuring Electrostatic Fields in Both Hydrogen-Bonding and Non-Hydrogen-Bonding Environments Using Carbonyl Vibrational Probes. *J. Am. Chem. Soc.* **2013,** *135*, 11181-11192.

(2) Chen, Y.; Morisawa, Y.; Futami, Y.; Czarnecki, M. A.; Wang, H.-S.; Ozaki, Y. Combined IR/NIR and Density Functional Theory Calculations Analysis of the Solvent Effects on Frequencies and Intensities of the Fundamental and Overtones of the C=O Stretching Vibrations of Acetone and 2-Hexanone. *J. Phys. Chem. A* **2014,** *118*, 2576-2583.

(3) Hamm, P.; Zanni, M. *Concepts and Methods of 2D Infrared Spectroscopy*. 1st ed.; Cambridge University Press: Cambridge, UK, 2011.

(4) Schneider, S. H.; Boxer, S. G. Vibrational Stark Effects of Carbonyl Probes Applied to Re-interpret IR and Raman Data for Enzyme Inhibitors in Terms of Electric Fields at the Active Site. *J. Phys. Chem. B* **2016,** *120*, 9672-9684.